NASA/TM-1998-206288

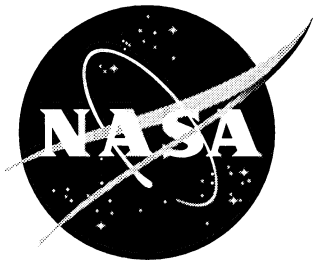

Hydrostar Thermal and Structural Deformation Analyses of Antenna Array Concept

Ruth M. Amundsen and Drew J. Hope
Langley Research Center, Hampton, Virginia

National Aeronautics and
Space Administration

Langley Research Center
Hampton, Virginia 23681-2199

February 1998

Available from the following:

NASA Center for AeroSpace Information (CASI)
800 Elkridge Landing Road
Linthicum Heights, MD 21090-2934
(301) 621-0390

National Technical Information Service (NTIS)
5285 Port Royal Road
Springfield, VA 22161-2171
(703) 487-4650

Table of Contents

Figures

Tables

Abstract

The proposed Hydrostar mission used a large orbiting antenna array to demonstrate synthetic aperture technology in space while obtaining global soil moisture data. In order to produce accurate data, the array was required to remain as close as possible to its perfectly aligned placement while undergoing the mechanical and thermal stresses induced by orbital changes. Thermal and structural analyses for a design concept of this antenna array were performed. The thermal analysis included orbital radiation calculations, as well as parametric studies of orbit altitude, material properties and coating types. The thermal results included predicted thermal distributions over the array for several cases. The structural analysis provided thermally-driven deflections based on these cases, as well as based on a 1-g inertial load. In order to minimize the deflections of the array in orbit, the use of XN70, a carbon-reinforced polycyanate composite, was recommended.

Introduction

There have recently been several programs at NASA Langley Research Center involving design of large orbiting antenna arrays for synthetic aperture radiometer measurements[1,2,3]. ICESTAR was a proposed microwave radiometer array to measure and track large-scale movements of ice ridges and leads over the North Pole regions to facilitate sailing and shipping via a polar sea route[4]. ESTAR was a proposed array to measure soil moisture from a satellite platform[5]. Some detailed thermal analysis was performed for ESTAR to evaluate the stability for waveguide-mounted electronics[6]. Hydrostar was a proposal for a joint mission by NASA Goddard Space Flight Center and NASA Langley Research Center (as well as several other industrial collaborators). The Hydrostar mission objective was to demonstrate synthetic aperture technology in space while obtaining global soil moisture data[7].

One of the most challenging requirements on any of these arrays is that, to take accurate measurements, the array must remain planar and well aligned while in orbit. This means that the separate waveguide elements must not move or twist in relation to each other, and must also accurately retain their own original shape. There are two types of requirements on the array stability. The first is that the array elements must be within some tolerance of their ground-test positions when the array is initially deployed on-orbit. This is the initial deployment accuracy, and the stringency on this requirement will depend on how well an initial on-orbit calibration[8,9] can be performed. The second type of requirement is on changes over an orbit, i.e., the orbital stability. The level of this requirement will depend on whether calibrations can be done as frequently as once per orbit, and how much motion of the waveguides can be tolerated and still carry out a successful calibration. For each class of stability requirement, there will be six tolerance values -- one for each axis of translation and rotation. In addition, there may be different tolerances on the motion of waveguides close to each other (e.g., tolerance on relative motion of first to second waveguide) as opposed to waveguides that are far apart (e.g., first to last waveguide). All of these position requirements will also be affected by the required accuracy and measurement resolution of the array. Another potential requirement is that the array should remain relatively stable in temperature over the course of a year, as well as over the course of an orbit. For the Hydrostar program, these requirements were not yet completely specified at the time the thermal and structural analyses were performed. However, an order-of-magnitude number of less than one centimeter of motion was defined as a starting point. The angular rotation tolerance was about 1 degree. More specific values were roughly set at the following: initial deployment spacing accuracy of 2 mm for closest waveguides and 2 cm for most distant waveguides; orbital stability out-of-plane 1 cm and in-plane 5 mm/m. These requirements would need to be completely determined before final analysis of a flight design antenna was performed.

The baseline Hydrostar array consisted of 16 waveguide elements that were each 5.8 meters in length. The full array deployed to a width of 9.8 m. Each array element, or waveguide, had a hollow rectangular cross-section of 16.9 cm x 8.6 cm. The wavelength (λ) used was 10.7 cm. The large dimensions of the overall array, and the relatively small sizes of the waveguide walls, led to interesting challenges in modeling, as discussed below.

Both thermal and structural analyses were performed on the baseline Hydrostar array concept to define the maximum deformations predicted as a result of thermal gradients. An orbital analysis was performed to define the orbital fluxes on the surfaces of the array elements and support truss. Several parametric analyses were performed in an attempt to determine the optimum surface coating for thermal objectives. A thermal analysis was performed using the orbital fluxes, to define the thermal gradient over the entire array and to predict the thermal transient

over the course of an orbit. Finally, several structural analyses were performed using the predicted temperature distributions, to predict on-orbit deflections due to the thermal variations. Several different materials were evaluated for their performance both thermally and structurally.

Orbital Analysis

The projected orbit for the array was used to define the worst-case orbital flux variations that might be seen. The orbital parameters were a sun-synchronous orbit with a 6 a.m. ascending node launch in the year 2000, and potential orbital altitudes of 420, 500 and 675 km. These parameters give maximum and minimum potential β (beta) angles of 89.7° and 58.5°, respectively, as shown in Figure 1. These will be referred to as the β 90 and β 60 orbits, although the exact values were used in analysis. The orbit period is 1.5 to 1.6 hours, depending on the altitude. Figure 1 also shows that the orbit altitude has little effect on the minimum and maximum β angles; candidate altitudes of 420, 500 and 675 km are plotted, with negligible effect on the β angles. The β angle definition used here is the angle between the orbit plane and the solar vector. The Sun-synchronous Orbit Analysis Program (SOAP)[10] was used to perform these calculations.

In the near-90° β angle case, the orbiting array never passes into a shadowed part of the orbit, while in the near-60° case it is in shadow for 18 to 26% of the orbit, depending on altitude. Progression into and out of shadow will obviously cause the most severe thermal transients. If it were desirable from an instrument science point of view to always avoid the most severe transients, the operation of the instrument could be restricted to full-sun (unshadowed) orbits only. If this were the case, there would be 252 full-sun operable days per year at 420 km, 262 days per year at 500 km, and 278 days per year at 675 km altitude. The percentage of the orbit when the array is in shade is shown in Figure 2 for the entire range of β angles and all three altitudes.

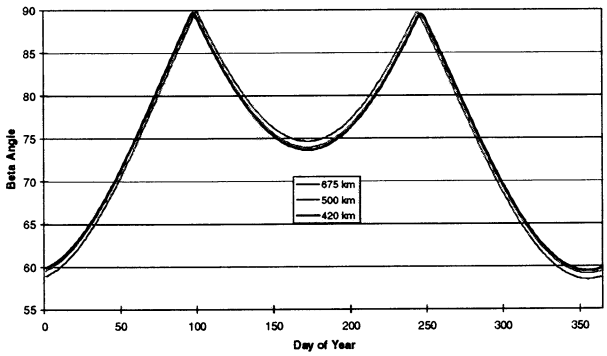

Figure 1. β Angle Variation for Several Orbit Altitudes

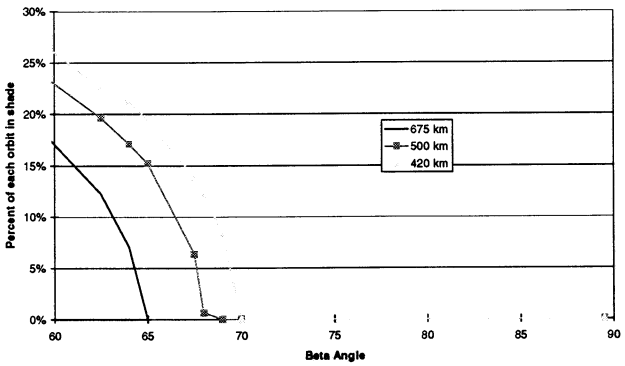

Figure 2. Shade in Orbit versus β Angle and Altitude

Parametric Evaluations

Radiative Analysis of Coatings

Based on the above range of β angles, test cases were run to roughly determine the optimum thermal coatings for the antenna elements. Models were developed in TRASYS (Thermal Radiation Analyzer System)[11] and SINDA-85[12] that included short sections of the first, second and fourth antenna elements. These elements were chosen to cover most of the types of shading present on the array. The first element was included to get the surface with full sun in the β 90 orbit, the second was included for the representation of the closest-facing surfaces, and the fourth adds the vertical surfaces that have intermittent shading. The TRASYS test case model is shown in Figure 3 with definitions of the surfaces. These models were used to evaluate both the thermal gradients across the elements and the transient over an orbit. The criteria were to minimize both gradient and transient in both the β 60 and β 90 orbits. Also, use of multi-layer insulation (MLI) blankets was kept to a minimum due to packaging problems. No MLI was allowed on earth-facing surfaces (the active side of the array), or on the sides of the elements which would be brought together when stowed. All coatings used are available in sheet form, with pressure adhesive backing, to facilitate application on the exterior faces of the antenna elements. On the Earth-facing (active) side of the antenna elements, an aluminum coating could be directly deposited, rather than using a polymer film and adhesive, to eliminate potential interference with the array performance. Several possible arrangements of coating properties were evaluated. Fluxes, gradients and transients were looked at for both extreme β angle orbits. The properties used in the evaluation are shown in Table 1. Degraded properties were used in the full array analyses. Because it was initially uncertain how much of the surface would be available for coating, and how much would be used for tape and penetrations, the slightly altered values shown were used for the test model. For surfaces where MLI was modeled, it was assumed to perform as a simple fraction of the emissivity and absorptivity; 5% of the values for the outer surface were used.

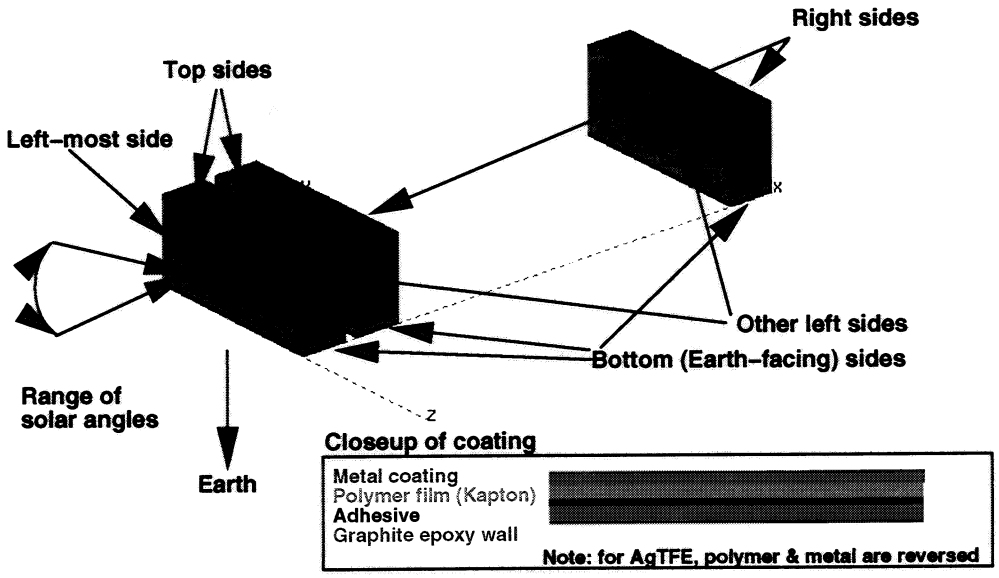

Figure 3. TRASYS Model for Coating Evaluation

Table 1. Optical Properties Used for Thermal Coatings

Material	Beginning of Life α/ε	End of Life α/ε	Test model α/ε
7.5 mil Ag/TFE	0.1 / 0.8	0.15 / 0.8	0.15 / 0.8
VDA on Kapton	0.14 / 0.05	0.2 / 0.1	0.3 / 0.1
Kapton	0.5 / 0.77	0.5 / 0.8	0.3 / 0.8
SiO_2/Al/0.5 mil Kapton	0.14 / 0.12	0.15 / 0.15	0.15 / 0.15

The TRASYS model of this test case used only one surface per side of each waveguide. This produced accurate TRASYS radiative results. However, in the SINDA-85 and P/Thermal[13] models, this assumption led to some inaccuracy in the predicted gradients. PATRAN P/Thermal models were only developed for the full array, and not for the test case. In the full array models, there was still only one node or surface defined across the width of each side of the waveguide, although there were many nodes along the length. The reason the models were kept at such a relatively coarse mesh was to stay within the TRASYS overall limit on number of surfaces. For the SINDA models, there will not be much error in the gradients, since the lumped node is in the center of each side, and thus conductance and TRASYS heat input will be defined from the center of each side, and will be numerically correct. However, in the P/Thermal models, with the version of MSC/PATRAN used in this analysis (5.0), the nodes are defined as in a finite element model, at the corners of each element. Thus, the heat fluxes and radiation to space are apportioned to the corners, and some of the driving forces for the gradients are lost. Basic conclusions and trends can still be drawn from this analysis, although a more detailed model should be done if this analysis is to be used for flight hardware design. A more detailed model can be done using this analysis method by applying the TRASYS fluxes from a coarse mesh model to a more detailed finite element model, i.e., each TRASYS flux is applied to several finite elements. However, because of the dimensions and number of the waveguides, more finely dividing the mesh quickly drives the model to an unwieldy size.

Seven different optical coatings were evaluated; the seven coatings consisted of the four coatings in Table 1, and each one as the outer layer of an MLI blanket (except for the vapor deposited aluminum). First, a TRASYS model was run for each as the sole coating on all surfaces of the test model. For each case, the heat flux input from solar, Earth albedo and Earth IR was summed on each surface. Then the amount of heat lost to space via radiation was subtracted, leaving the effective net power gained or lost by that surface, as an orbit average. This was done for both 60 and 90° β angle orbits. An example of this calculation is shown in Table 2.

Table 2. Example TRASYS Test Case Results

Surface Property, α/ε	**.15/.8**				**.15/.8**			
Orbit	**beta 60**				**beta 90**			
	Q input (Btu/hr)	**Rk to space**	**Q output (Btu/hr)**	**Difference (Btu/hr)**	**Q input (Btu/hr)**	**Rk to space**	**Q output (Btu/hr)**	**Difference (Btu/hr)**
Surface								
WG1 right	6.70	0.07	7.03	-0.3	2.25	0.07	7.03	-4.8
WG1 base	59.10	0.25	24.94	34.2	54.00	0.25	24.94	29.1
WG1 left	58.46	0.50	49.13	9.3	81.24	0.50	49.13	32.1
WG1 top	10.26	0.25	24.94	-14.7	0.04	0.25	24.94	-24.9
WG2 right	18.48	0.49	48.22	-29.7	16.52	0.49	48.22	-31.7
WG2 base	59.10	0.25	24.94	34.2	54.00	0.25	24.94	29.1
WG2 left	8.08	0.07	7.03	1.1	2.26	0.07	7.03	-4.8
WG2 top	10.26	0.25	24.94	-14.7	0.04	0.25	24.94	-24.9
WG3 right	17.09	0.50	49.13	-32.0	16.43	0.50	49.13	-32.7
WG3 base	59.10	0.25	24.94	34.2	54.00	0.25	24.94	29.1
WG3 left	58.07	0.49	48.22	9.9	16.96	0.49	48.22	-31.3
WG3 top	10.26	0.25	24.94	-14.7	0.04	0.25	24.94	-24.9

In order to calculate the heat lost to space, a temperature for the entire array had to be assumed. This will be dependent not only on the optical properties on the surfaces, but also on electronics self-heating, spacecraft temperature and operational scenarios. In fact, the decision might be made to use resistance heating to hold the array at a warmer temperature than it would normally attain. Since the array temperature could not be known at this point, the cases were run for several different assumed array temperatures to discern the impact that variable would have. Four different array temperature cases were run for each surface type and each orbit case: -70°, -50°, -20° and 0°C. Only two of these temperature cases are shown, since all led to roughly the same results.

The effective heat gained or lost by the surface ($Q_{net} = Q_{in} - Q_{out}$) was averaged for the β 60 and β 90 orbits as a root-mean-square [$Q_{avg} = (Q_{in}^2 + Q_{out}^2)^{1/2}$], since some net heating values were negative. This averaging allowed selection of a coating that is optimized over the entire range of β angles. The number of effective surfaces was reduced from twelve to five, by averaging together similar surfaces that would probably receive the same coating (e.g., all top surfaces averaged). This was done since the results for same-facing surfaces were similar, and the use of similar coatings on equivalent waveguide surfaces facilitates manufacturing and assembly. The only exception was that the left-most surface was kept separate, as it is the only left-hand surface to receive full sun, and consequently might be the only one to receive a different coating. Thus the averages are: all right sides (away from the sun), all Earth-facing sides (bases), all tops, the sun-most (outer-most) left side, and all other left sides.

The objectives for the optimum coatings are as follows:

(1) The differences in net heating between surfaces should be as small as possible, in order to minimize the thermal force driving the waveguide gradients. In other words, a coating should be selected for each surface that results in the net heating values for all surfaces being as close to equal as possible.

(2) The change in heating rates over the course of an orbit should be as small as possible, to optimize the orbital temperature stability.

(3) The difference in net heating between the β 60 and β 90 orbits should be as small as possible, to minimize the temperature change over the year.

Figure 4 shows the net effective heating rates for all the coating types for a -50°C array temperature, and Figure 5 shows the same for a 0°C array temperature. These figures were used to select the coating test cases shown in the next section. The differences between the β 60 and β 90 orbits for each coating type are shown in Figure 6. The changes in fluxes over an orbit for each coating type were also calculated. The standard deviation in heating over an orbit and the maximum heating change over an orbit were both averaged over all waveguide surfaces. This is shown in Figure 7, only for the β 60 orbit, since the β 90 orbit does not have much variation. It can be seen that the AgTFE and Al-SiO_2 have much lower deviations around an orbit, since they have lower α and thus pick up less solar heating. Obviously, the MLI-covered surfaces have much less deviation since they are better insulated.

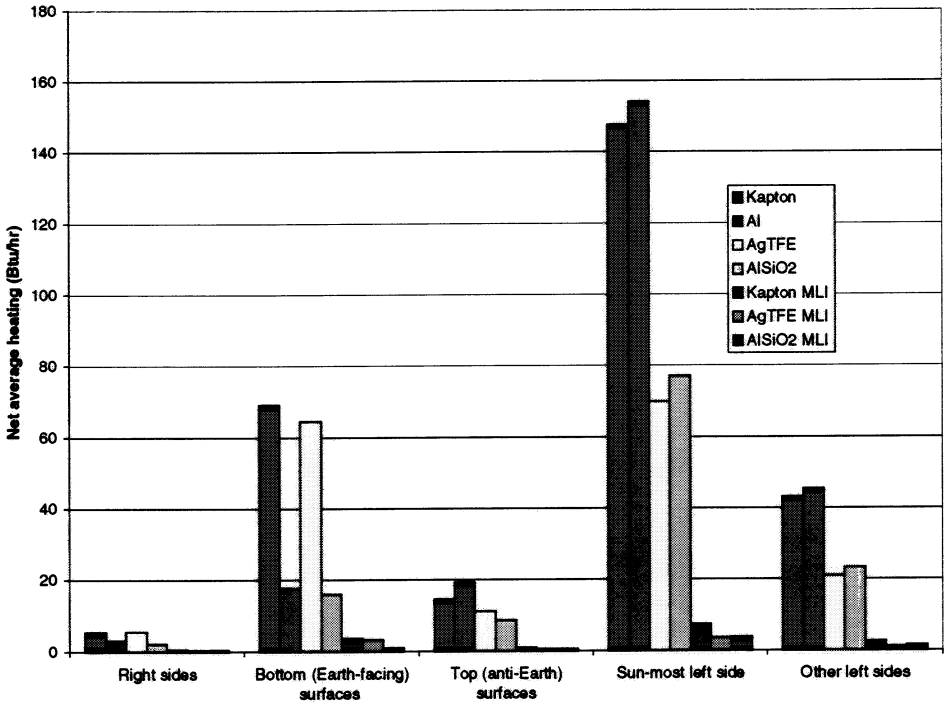

Figure 4. Net Heating for Coatings (-50°C array, β 60 and β 90 averaged)

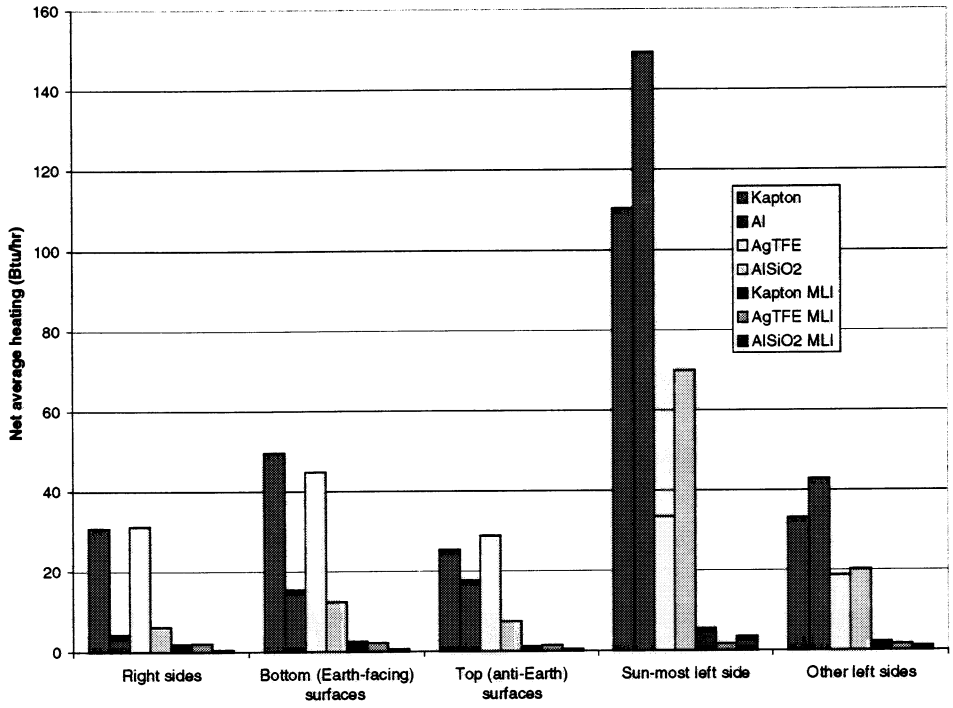

Figure 5. Net Heating for Coatings (0°C array)

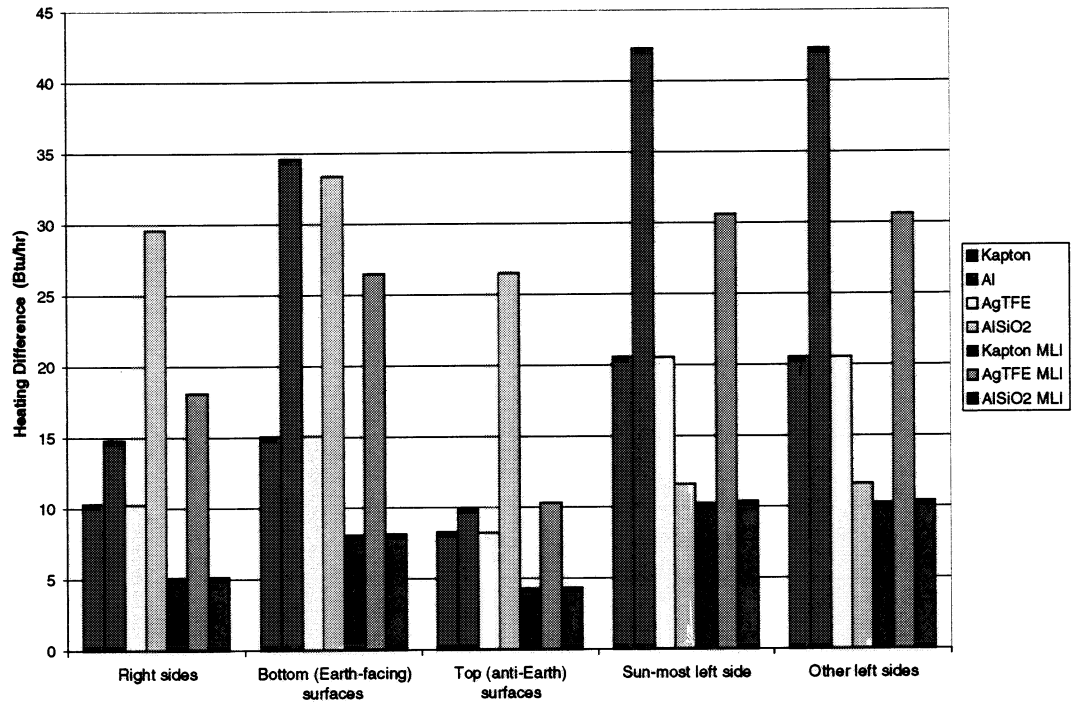

Figure 6. Heating Differences between β 60 and β 90 Orbits (Averaged over Orbit)

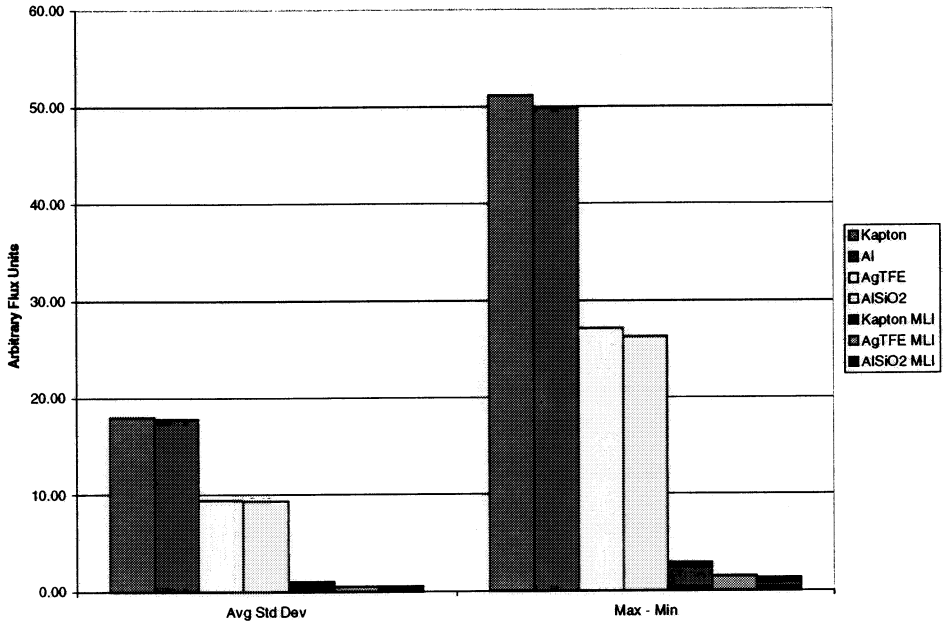

Figure 7. Standard Deviation and Range of Fluxes over a β 60 Orbit

Thermal Analysis of Test Cases

The values produced in the TRASYS analysis of the coatings were used to construct two test cases for the entire array's coating scheme. These test cases were run in both TRASYS and SINDA to make thermal predictions of gradients and transients. The coatings used for the two cases are shown in Table 3 and Table 4.

Table 3. Case A Coating Arrangement

Surface	Coating	Rationale
Right sides	Aluminum	Simplest to apply, lowest average differences
Earth-facing sides	Aluminum	Must be used on active face
Top sides	Al-SiO_2 MLI	Limits large heat gain
Sun-most left side	Kapton MLI	Limits large heat gain and mitigates difference between β 60 and 90 orbits
Other left sides	Al-SiO_2	Lowest differences of non-MLI coatings evaluated

Table 4. Case B Coating Arrangement

Surface	Coating	Rationale
Right sides	Kapton	Best for handling
Earth-facing sides	Aluminum	Must be used on active face
Top sides	Kapton MLI	Limits large heat gain, best for handling
Sun-most left side	Kapton MLI	Limits large heat gain and mitigates difference between β 60 and 90 orbits
Other left sides	Al-SiO_2	Lowest differences of non-MLI coatings evaluated

The fluxes from the TRASYS runs on Case A and Case B were used to determine which set of coatings would give the best results -- the most uniform and stable temperatures. Cases A and B were run for both β 60 and β 90 orbits, both steady-state and transient. Table 5 shows the average temperature across all surfaces for the steady-state (or orbit-average) runs, and the standard deviation (dispersion from the mean) of those temperatures. Case A has slightly warmer temperatures, and the standard deviation is roughly equivalent for Cases A and B. Figure 8 shows that Case A has the larger difference between the β 60 and β 90 orbits, but that the standard deviation in temperatures across the waveguides, averaged between the β 60 and β 90 orbits, is almost exactly equal. Figure 9 shows the maximum gradients across each waveguide section for each of the four cases. On each of the three test waveguide sections, for both β 60 and 90 cases, Case A has lower gradients.

Table 5. Case A and B Orbit-Average Results

Case / orbit	Average temperature (°C)	Standard Deviation of Temperatures
Case A, β 60	22.8	19.6
Case A, β 90	-48.3	22.8
Case B, β 60	-16.4	25.1
Case B, β 90	-66.5	17.0

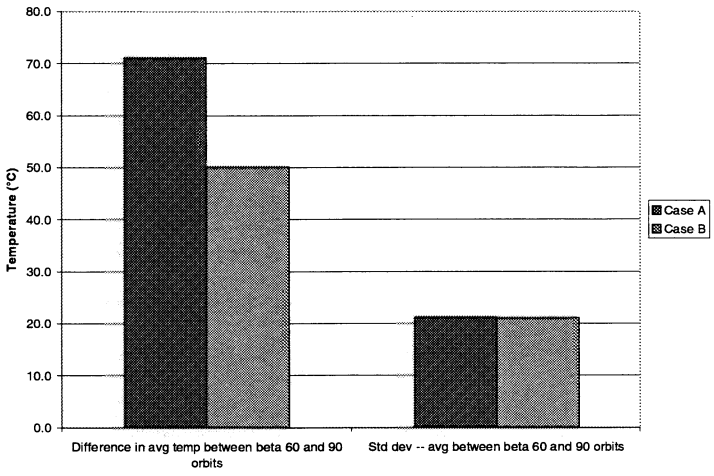

Figure 8. Comparison of Cases A and B

Transient cases over an orbital time period were run for all four conditions (Cases A and B, orbits β 60 and β 90). An example table of results from one of these runs is shown in Table 6. The temperature of each waveguide (WG) surface is calculated around an entire orbit, starting from initial temperatures defined by the orbit average steady-state case. The last two columns show the average temperature across the entire test model and the standard deviation of temperatures across the model. Two values that condense the performance of the model are calculated from the last two columns. The standard deviation in the average temperatures is an indication of the transient stability (in other words, how much the average changes with time, or the mean of thermal dispersions over an orbit). The average of the standard deviations is a measure of the overall gradient (how much variation in temperature there is across the array). These two defining values were calculated for each test case. These values are shown in Table 7. As can be seen by comparing the values for each orbit, these generalized performance measures do not show much difference between Cases A and B. However, a difference in the two coating schemes can be observed by plotting the gradients across each waveguide. This is done in Figure 10, which shows the maximum

gradient at any point in the orbit across each of the three waveguide test sections, the maximum gradient across any single waveguide and the maximum gradient across the entire array. In all of these measures, the Case A coating scheme performs better for both β 60 and β 90 orbits. Figure 11 also demonstrates that Case A is preferable by showing the average and maximum change in temperature of any waveguide surface over the course of an orbit.

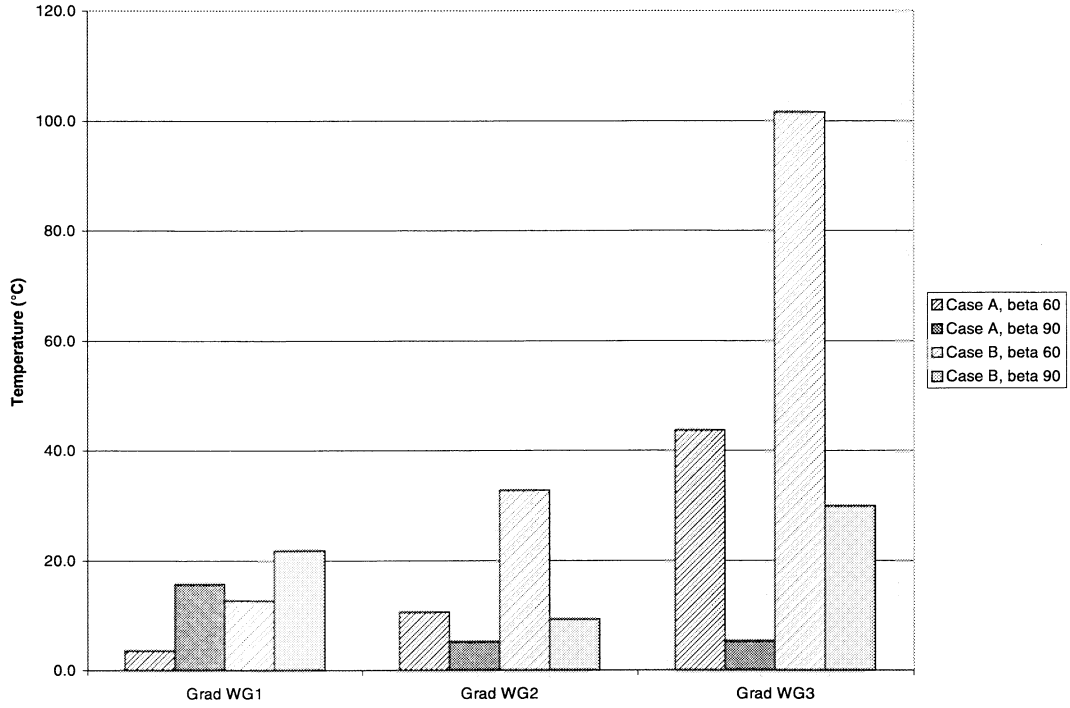

Figure 9. Maximum Waveguide Gradients for Orbit Average Cases

Table 6. Example Transient Test Case (Case A, β 60 orbit, 420 km altitude -- all values in °C)

Time (hrs)	WG1 right	WG1 base	WG1 left	WG1 top	WG2 right	WG2 base	WG2 left	WG2 top	WG3 right	WG3 base	WG3 left	WG3 top	Avg. Temp.	Std. Dev.
0.0	26.0	28.9	25.7	25.3	-5.0	5.7	1.3	-2.1	20.2	42.1	64.0	41.3	**22.8**	**19.6**
0.2	31.9	33.3	28.0	28.0	-1.2	10.0	5.5	0.5	23.3	47.6	76.8	45.2	**27.4**	**21.5**
0.4	30.0	28.3	29.3	28.6	-1.5	5.1	4.6	1.2	23.5	45.2	80.7	48.7	**27.0**	**22.7**
0.6	30.7	45.0	30.8	28.8	-1.9	21.4	5.5	0.8	24.4	62.7	82.7	50.3	**31.8**	**24.2**
0.8	23.7	26.7	26.3	27.2	-5.4	3.3	0.7	-0.5	23.5	38.9	41.2	42.9	**20.7**	**16.3**
1.0	17.2	18.3	20.8	22.7	-10.1	-4.6	-4.7	-4.2	17.2	23.1	20.2	29.7	**12.1**	**13.2**
1.2	20.8	23.4	22.7	20.6	-9.3	0.5	-2.7	-6.3	12.6	29.0	53.4	27.5	**16.0**	**17.3**
1.4	19.1	24.4	23.5	21.4	-7.5	1.1	-4.3	-5.7	13.3	35.3	68.0	33.9	**18.6**	**20.7**
1.6	31.8	31.4	25.3	24.6	-3.4	8.1	4.4	-2.8	18.8	45.9	76.8	41.4	**25.2**	**22.0**
1.8	31.1	33.6	28.2	28.5	-0.5	10.3	4.9	1.0	23.1	49.5	81.6	47.4	**28.2**	**22.7**
2.0	30.5	28.6	29.3	28.8	-1.8	5.3	4.9	1.2	23.5	46.5	82.4	50.2	**27.4**	**23.2**

Table 7. Case A and B Performance Measures

Case	Standard Deviation of Averages (transient stability) -- in °C	Average of Standard Deviations (gradient) -- in °C
Case A, β 60	5.7	20.3
Case A, β 90	0.3	22.5
Case B, β 60	5.9	25.8
Case B, β 90	0.3	18.7

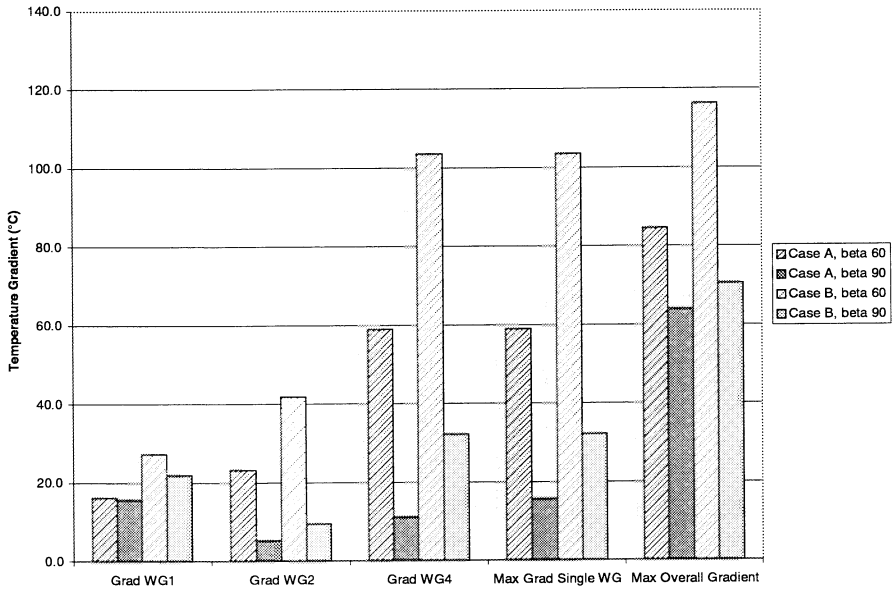

Figure 10. Maximum Waveguide Gradients for Cases A and B (Transient Analysis)

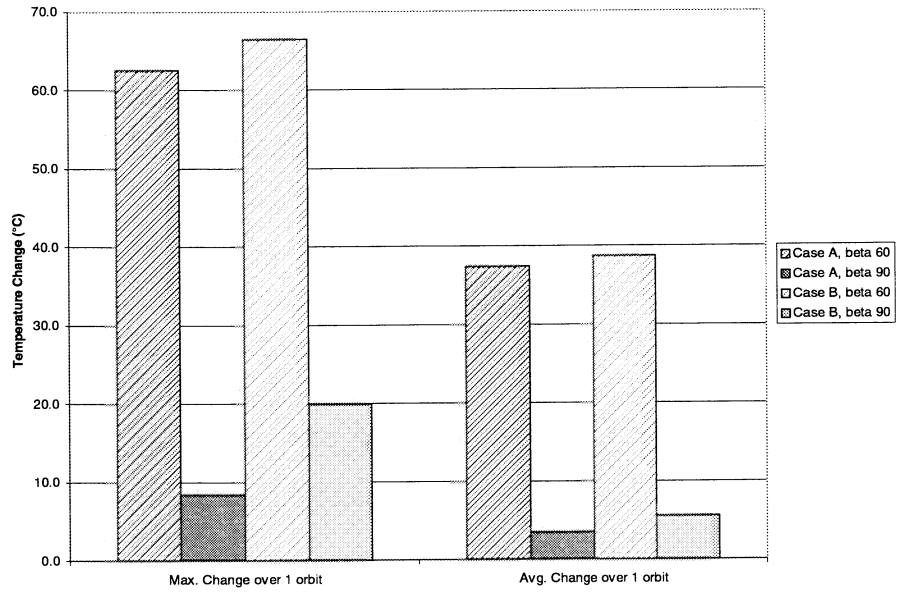

Figure 11. Waveguide Transients for Cases A and B

Graphite-Epoxy Conductivity Evaluation

Coating Case A (for both steady-state and transient cases, both β 60 and 90 orbits) was run for two types of graphite-epoxy, to evaluate the effect of different material thermal conductivities. The two composites used for comparison were T50/934 (normally has a thermal conductivity of about 20 W/mK, 10 W/mK was used for continuity with earlier work[7]) and P75/1962 (52 W/mK)[14]. As can be seen in Figure 12, an increase in the thermal conductivity of the waveguide material has a much more substantial impact in decreasing the gradients than a change in surface coatings. For these two materials, the gradients are cut by a factor of four or five -- the same as the difference in their thermal conductivities. The generalized performance measure used earlier, the average of the standard deviation of temperatures across the test section (Figure 13) shows that the higher k composite gives better values for each orbit case. Also, as shown in Figure 14, the transients are reduced significantly.

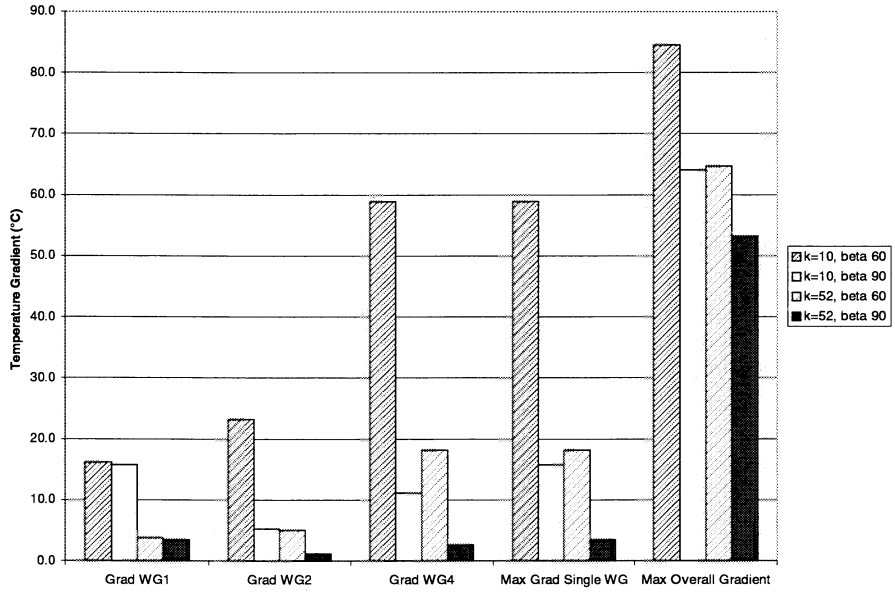

Figure 12. Gradients for Thermal Conductivity (k) Comparison

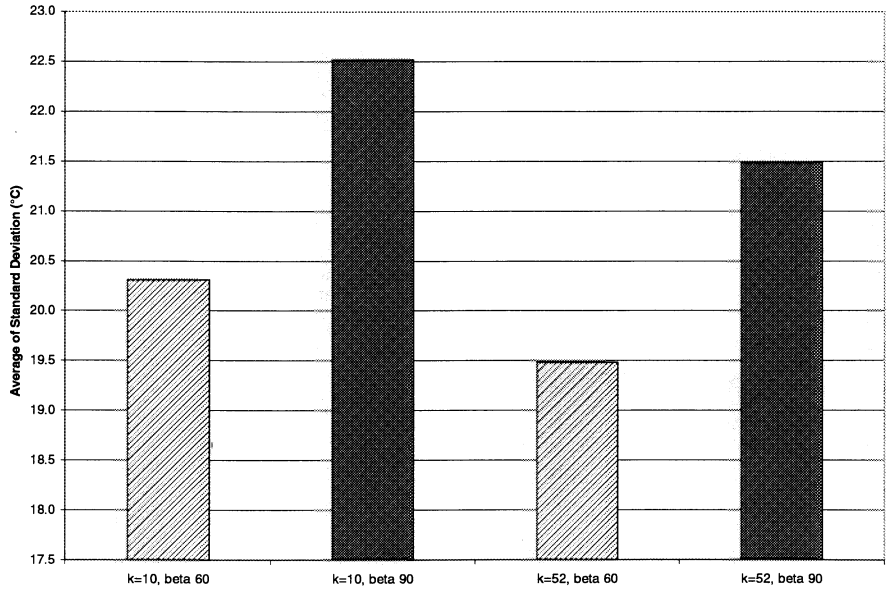

Figure 13. Comparison of Performance for k Variation

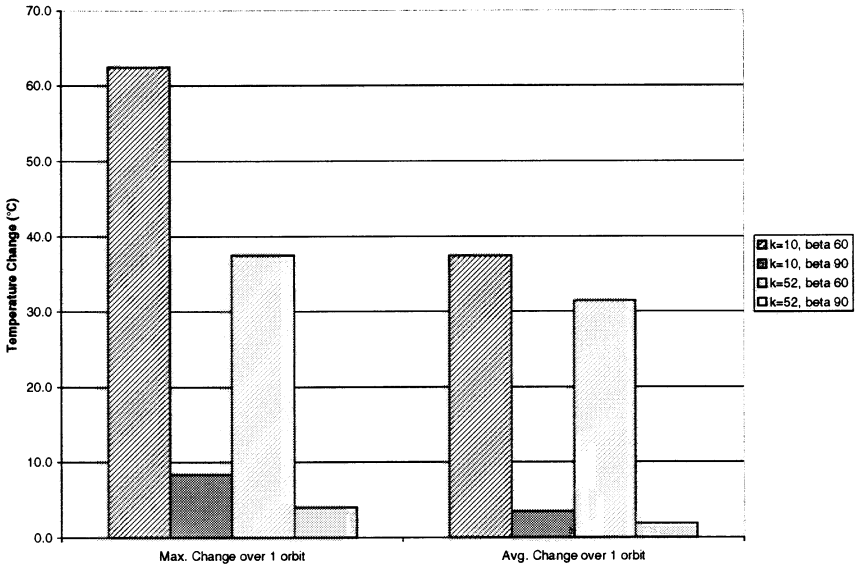

Figure 14. Waveguide Transients for k Comparison

This evaluation of coatings and materials was not exhaustive – the optimization should be re-run when the array is in the preliminary design phase and more is known about where MLI can be used, what array temperature is required, and the exact orbit. The preceding analysis is shown in detail to illustrate the method for selecting the optimum coating combination and waveguide material.

Thermal Analysis of Array

Assumptions

For the analysis of the entire array, it was assumed as a worst-case that MLI could not be used in any location, and that all coatings had to be a single layer applied with adhesive or direct-deposited. Since MLI was not employed, AgTFE was used as the coating on the top surfaces, to minimize the absorption of solar input. The coating arrangement used was silver-Teflon (AgTFE) on the top (zenith) surfaces, SiO_2-coated aluminum on the side faces, and vapor-deposited aluminum (VDA) on the bottom (Earth-facing) sides. This is not an optimized coating scheme, but was used for this case since (1) not enough parameters were known to fully optimize the coatings, and (2) a high *k* graphite epoxy, which had been observed to make at least as much improvement as coating optimization, was used. The orientation of the full array is shown in Figure 15.

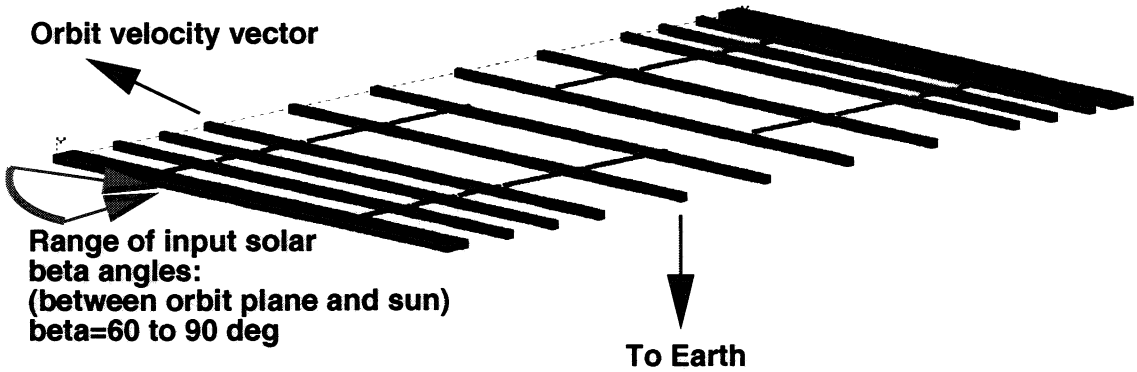

Figure 15. TRASYS Model of Array

With these surface properties selected, an analysis of the entire array was performed. A PATRAN model of the array was generated based on a WR650 waveguide cross-section. The array elements were 16.9 cm x 8.6 cm in cross-section, with a wall thickness of 0.15 cm. Each element was 5.8 m in length, and the array was deployed to its full extent of 9.8 m. Two simple struts (made of the same material as the waveguides) were assumed between each antenna element, each 7.6 cm in diameter with 0.64-cm wall thickness. The PATRAN model was translated to TRASYS to run the orbital fluxes, and these fluxes were input back to P/Thermal (the PATRAN thermal analyzer module) for a solution. The entire model consisted of 2714 nodes. For thermal purposes, simple steel pins were used as the connection between the array elements and supporting struts. If the antenna elements were slightly different in shape, as has been proposed, this would probably have little effect on the analysis results.

The TRASYS portion of the model was limited to 2000 nodes. When the model was transferred from P/Thermal to TRASYS, all surfaces were translated as the 'POLY' type. These were manually changed to 'RECT' surface type before running the TRASYS model to facilitate the model solution (additional details on methods can be found at Web address http://amsd-www.larc.nasa.gov/amsd/refs/des_analysis.html). Surface properties and orbital parameters were defined as stated earlier.

The mass and power of the front-end electronics box mounted on each element were neglected. An earlier study looked at methods for stabilizing electronics temperatures for a similar mission[6]. Judicious use of coatings as radiators for the boxes, the thermal mass of the boxes themselves, and isolation of the boxes from the elements could all be used to stabilize the electronics box temperatures and limit their effects on the antenna elements. Thus it was considered justifiable to neglect them. The mass of the electronics boxes would also act to mitigate transient effects, which should mean that the transient analysis here is conservative. Also neglected was the shading from the spacecraft and solar arrays on the antenna array. At the time of the modeling, not enough was known about the spacecraft to model it accurately. This was not felt to be a substantial omission, since the coatings and/or position of the spacecraft in the deployed configuration can probably be modified if necessary to mitigate any effects. Also, the thermal mass of the spacecraft will represent a stabilizing influence and would tend to decrease the transient changes seen over the course of an orbit.

Case Results

In order to capture all behaviors, a full spectrum of cases was run. The two extreme β angles were run for both an orbit-average (pseudo-static) case and for a transient case around an orbit. Three materials for the array were run for each case: aluminum alloy 7075, carbon-epoxy T50/934, and XN70, a carbon-reinforced polycyanate composite with high thermal conductivity. The lay-up and selection criteria are discussed later in the structural analysis section. To compare the materials' performance, the same thermal case, the β 90 orbit average case, was run with all three materials. The β 90 case gives the most extreme gradient across the array, since the sun is directly in line with the array and impinges mainly on the sun-facing side of the first waveguide. The orbit average case for the β 90 orbit gives about the same results as the transient, since the array never passes into shadow. The differences between the minimum and maximum temperatures for each case are shown in Table 8. The full thermal maps (in degrees C) for the array are shown in Figure 16, Figure 17 and Figure 18 for aluminum 7075, graphite-epoxy T50/934, and graphite-epoxy XN70, respectively. Additional thermal prediction images are available at http://amsd-www.larc.nasa.gov/hydrostar/therm_model.html. A slightly better gradient could be achieved in the aluminum case by selecting a higher conductivity aluminum. This was not done because it will not substantially affect the results, and the structural deflection analysis indicated that any aluminum alloy would have higher-than-desired deflections. The XN70 material has the best overall performance. The thermal conductivity of the XN70 material is 150 W/mK[14], compared to roughly 10 W/mK for the T50/934, so the gradient in this case is reduced.

Table 8. Total Array Thermal Gradient for 3 Materials

Material	**Thermal Gradient across array (Maximum - Minimum) °C**
Al 7075	70
T50/934 graphite epoxy	94
XN70 carbon-polycyanate	61

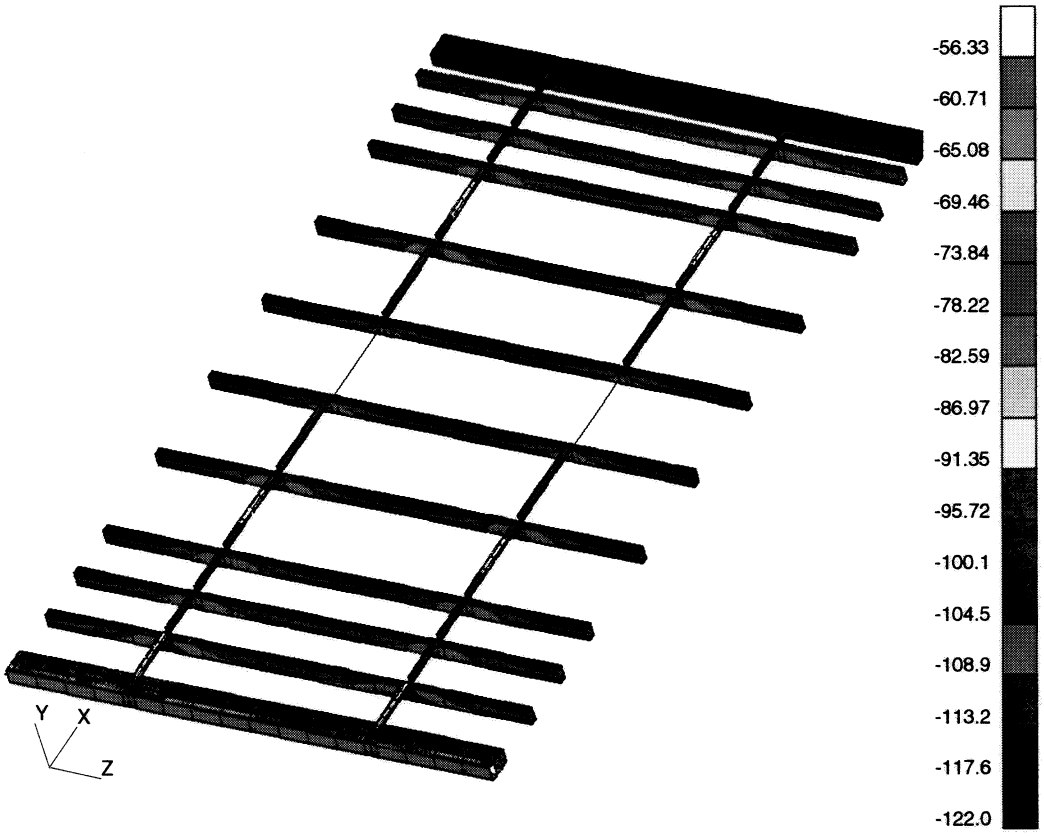

Figure 16. Orbit Average Case (β 90) for Al 7075

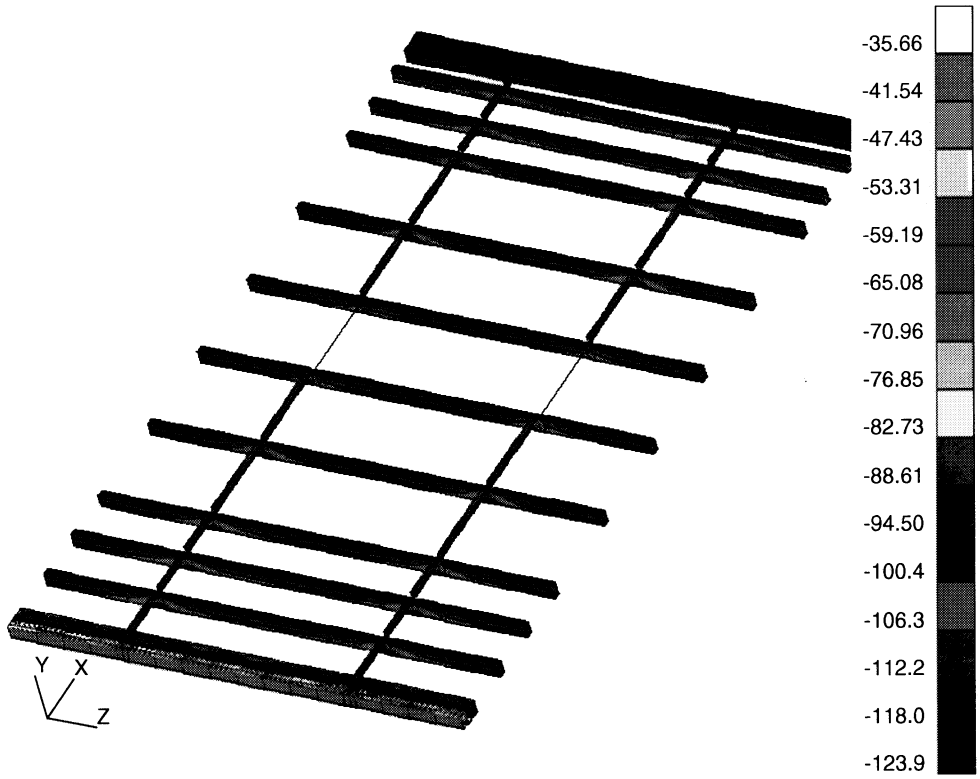

Figure 17. Orbit Average Case (β 90) for T50/934

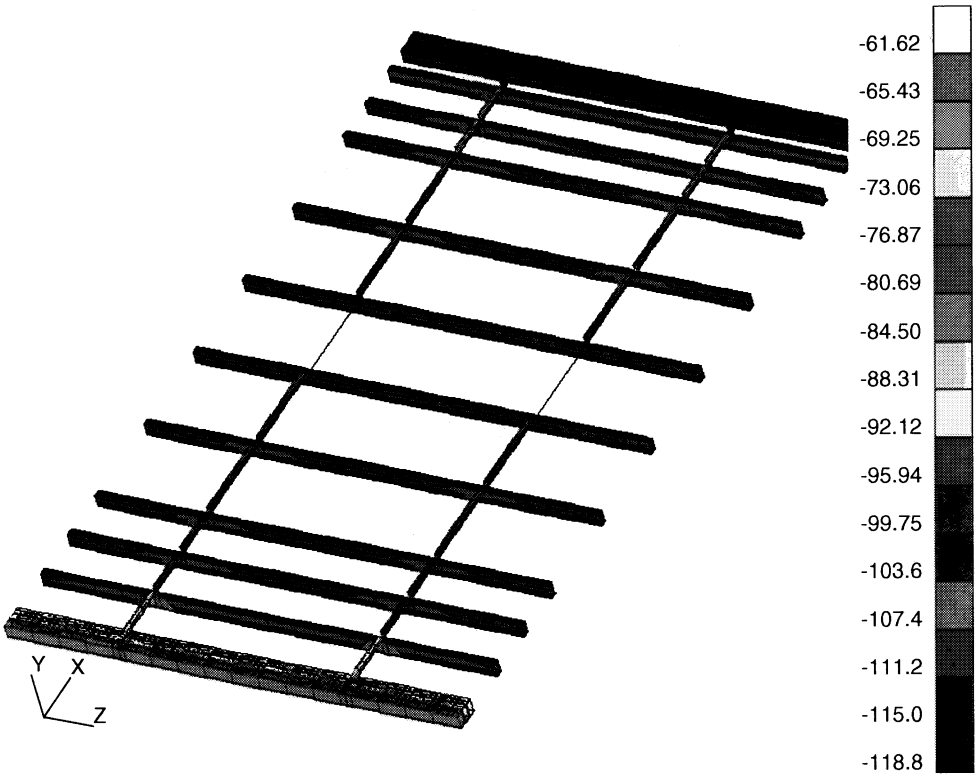

Figure 18. Orbit Average Case (β 90) for XN70

Runs with the XN70 material were used to show gradients in other orbit cases, as well as transients around an orbit. All of the following plots are shown with the final material selection, XN70 graphite epoxy. In the β 90 case, the static and transient cases both show a large gradient across the array, from element 1 to the other elements. This is due to the fact that nearly all the solar flux is impinging on the sun-facing side of the first element. This situation could be improved by using a small shade or MLI on the outermost sun-facing side. The static orbit-average case is shown in Figure 18. There is very little variation in temperature around an orbit, and the orbit-average case is very similar to the transient cases, since the array never passes into shadow. Thus the transient case is not pictured separately. A plot of the transient response for two points on the array is shown in Figure 19. In these plots, WG 1 is the first (left-most) element, and WG 16 is the last element (on the opposite side of the array). The total temperature change is less than 0.3°C over the course of half an orbit (total orbit period is 1.5 hrs).

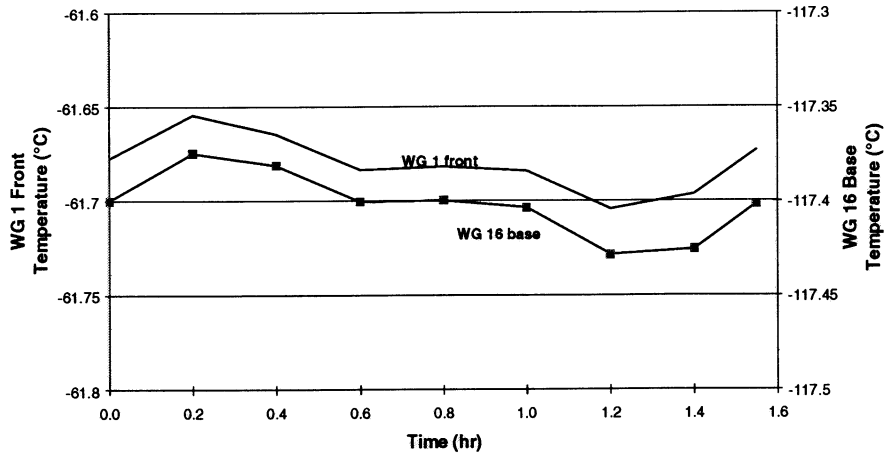

Figure 19. Transient Plot for XN70 -- β 90 Orbit

In the β 60 case, there is a substantial change over the course of the orbit, since the array is passing in and out of shadow. A plot of the transient response is shown in Figure 20. In this case, the orbit-average case is somewhat meaningless (since the changes are extreme), and instead a thermal map is shown at a specific point in the orbit (Figure 21). Some points on the array now undergo about a 30°C temperature change over the course of half an orbit. As can be inferred from the plot, the array goes into shadow in this case at about 0.6 hours, and comes out into the sun at about 1 hour (a 420 km orbit was used for these runs). As mentioned earlier, the actual transients would probably be less than this prediction, since in this model the thermal masses of the spacecraft, electronics boxes, and cabling are neglected. Also, the coating selection and placement could be optimized, or resistance heating could be used, to minimize both the gradients and transients experienced by the array.

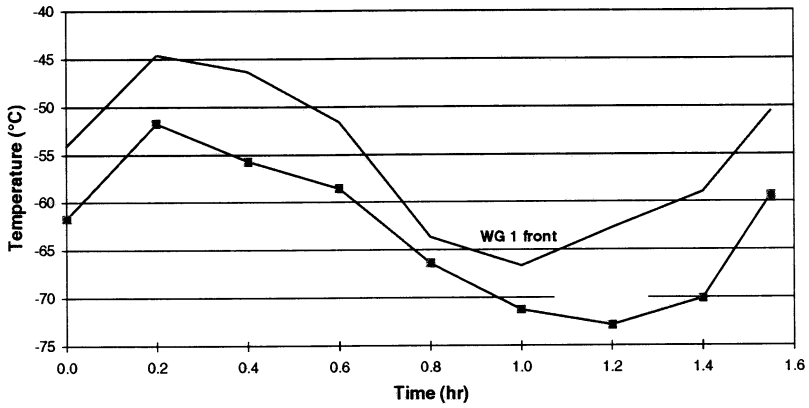

Figure 20. Transient Plot for XN70 -- β 60 Orbit

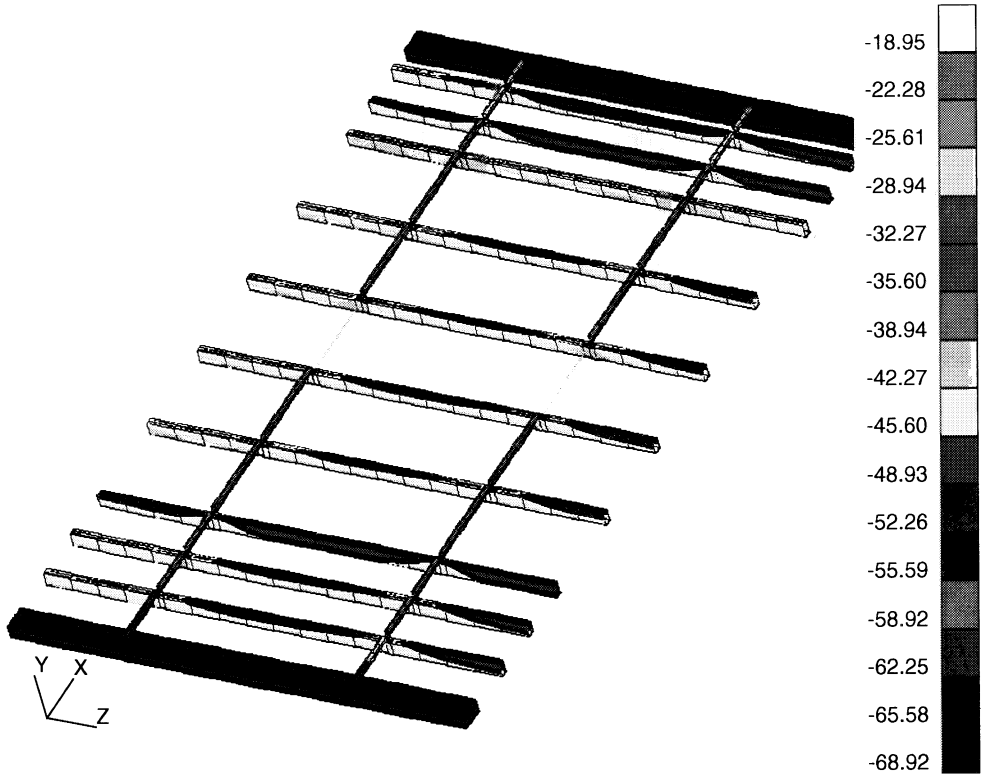

Figure 21. Thermal Gradient for XN70 in β 60 Transient Case (t = 0.8 hours)

Structural Analysis

Initially, a structural finite element model of the full array was created in MSC/PATRAN. In order to run parametric studies more rapidly, the model was simplified to two waveguides, without aperture slots, connected by two deployment elbows at the quarter span from each end of the waveguides, as shown in Figure 22.

The purpose of this model was to reduce the number of elements needed in the model, but still capture the deflections from the applied temperature gradients. By reducing the number of elements in the structural model, the complete antenna array could be modeled and analyzed with the TRASYS software, which had a limit of 4000 elements. The trial load cases applied to the model were a 20°C gradient from the top of waveguides to the earth-facing surfaces, and a 1g inertial load (due to operation in space after alignment in a 1g environment), as separate load cases. A Mechanica structural element model was created as a reference for determining the optimum number of elements in the PATRAN model. The PTC Pro/Mechanica[15] software is a structural and thermal analysis software package that uses geometric p-elements and automatically increases the order of the elements until solution convergence. A mesh density of 120 elements per waveguide in the PATRAN finite element model gave a solution that was within 5 percent of the Mechanica solution; this meshing was used.

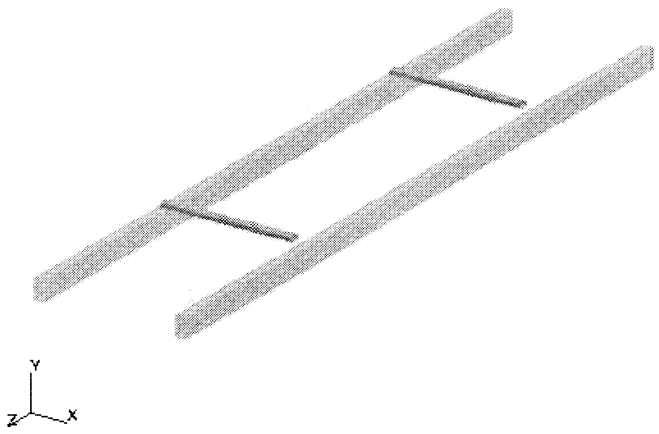

Figure 22. Simplified Two-waveguide Finite Element Model

The waveguides were each constructed with slots through the earth-facing surface that continued up the sides for a distance of 2.5 cm. The effect of these slots on deflections of the antenna structure needed to be determined. Models were developed both with and without slots using both aluminum 7075 and T50/934 graphite epoxy composite as the material. Figure 23 shows a detail view of the aperture slots in the finite element model.

The lay-up for the composites in the PATRAN model was a .005-inch thick ply in a 12-ply lay-up (60°, -60°, 0°, 0°, -60°, 60°) for the waveguides and a 24-ply lay-up for the deployment elbows. The connections between the deployment elbows and waveguides were represented by rigid connections (RBE2s) to transmit the translations at the end of the elbows into the waveguide structure. The results showed that the models with no aperture slots had an increased deflection of 15 to 25 percent for Al 7075-T651 and T50/934 graphite epoxy, respectively. The deflection results for Al 7075-T651 are shown in Figure 24 and Figure 25. This study showed that it was conservative to model the waveguides without slots, since the deflection prediction would be 15-25% too high. The decreased deflection when slots are present is believed to be due to the increased flexibility that allows decreased deflections by relieving contraction and expansion of the earth-facing sides of the waveguides from thermal loads. This conservatism allowed for some margin in modeling which was necessary in the joint area -- the connections between waveguides and deployment elbows were considered rigidly attached and there was no flexibility between deployment elbow joints, both of which are non-conservative assumptions.

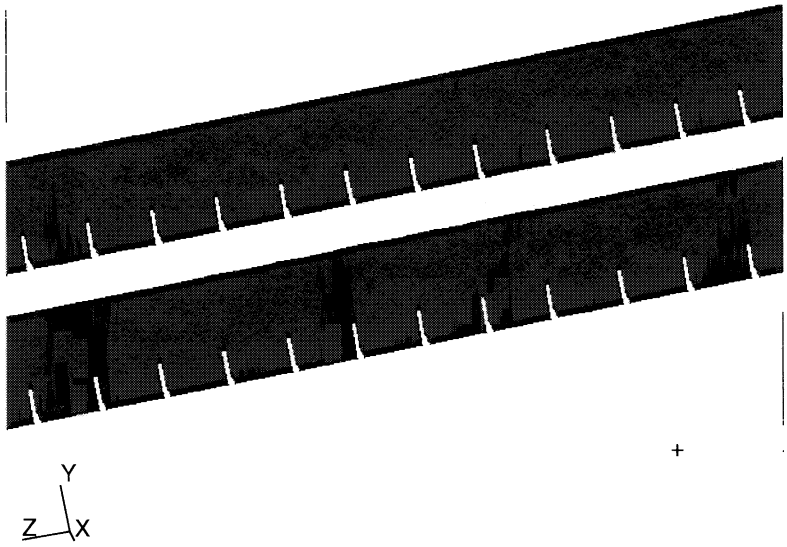

Figure 23. Detailed View of Two-waveguide Finite Element Model with Aperture Slots

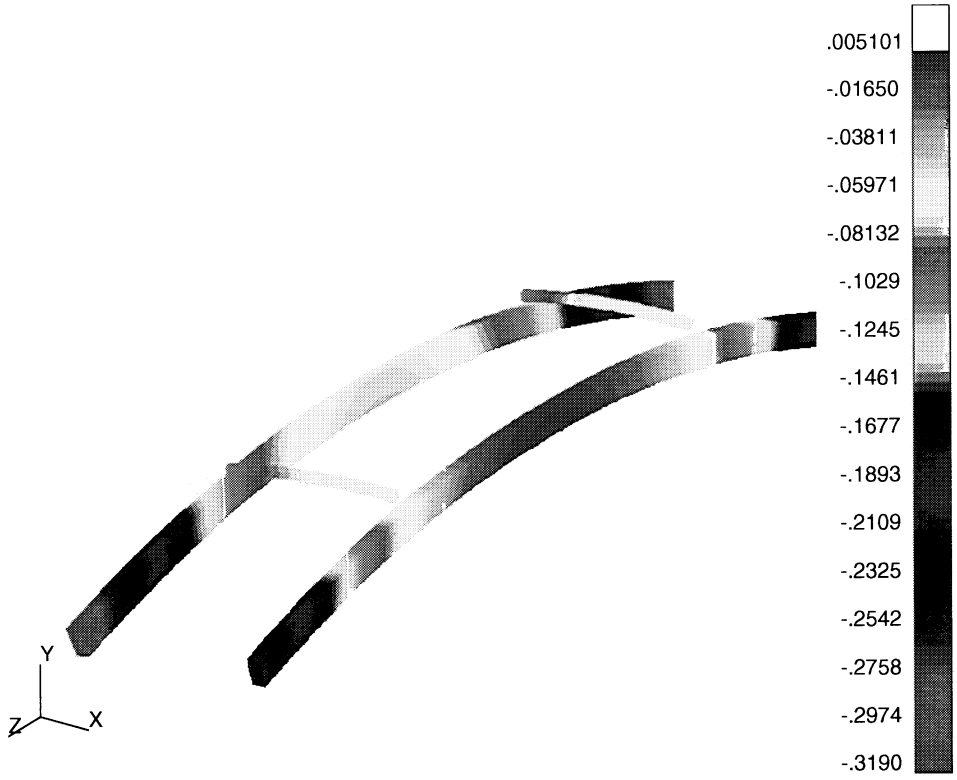

Figure 24. Deflections (inches) in Y-direction without Aperture Slots (Al 7075)

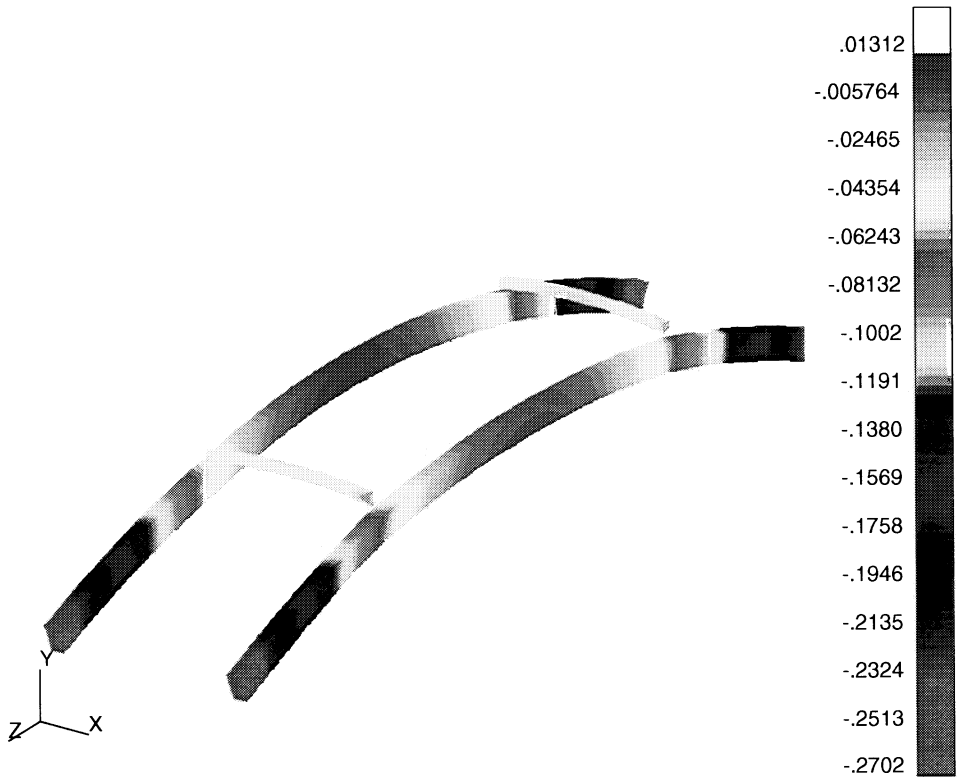

Figure 25. Deflections (inches) in Y-direction with Aperture Slots (Al 7075)

The structural analyses were then performed on the full antenna array, using the same PATRAN model employed in the thermal analysis, without slots. The Al 7075 and XN70 materials' deflection for both the β 90 static temperature gradient and orbit transient cases were compared. The lay-up for the composites in the full PATRAN model was the same as in the two-waveguide model. For Al 7075 the maximum deflection was 2.00 cm normal to the plane of the element array. The maximum out-of-plane deflections for the composite models were 0.95 cm for T50/934 carbon-epoxy composite and 0.003 cm for XN70. The property that has the most impact on the array deflection is the coefficient of thermal expansion (CTE or α), which is shown in Table 9.

Deformation analyses were performed using both Al 7075 and XN70 to determine the transient deflection in orbit. The orbit transient deflection is the maximum variation in deflection that occurs as a result of temperature changes around a β 60 orbit. The β 60 orbit transient deflections proved to be more severe than β 90 transient deflections due to the increased thermal transient over an orbit. The maximum transient deflection is 0.80 cm for Al 7075 and 0.004 cm for XN70 (shown in Figure 26). These deflections are based on the structure being perfectly constructed; i.e., there are no inaccuracies in the angle of layup or in the fiber angles, no asymmetry in the layer thicknesses, etc.

From the results of the deformation analyses, XN70 achieves the smallest deformations by a significant margin when compared with the Al 7075 and the T50/934 composite. Other properties that lend XN70 to space applications on arrays are that it is more resistant to microcracking than carbon/epoxy composites, which improves the dimensional stability, and that the lay-up of XN70 can be tailored so that the CTE of the composite is near zero.

Table 9. Material Properties

Property	XN70 Laminate	XN70 Lay-up (-60, 60, 0, 0, 60, -60)
α 11	-0.6 x 10^{-6} in/in/°F	-0.238 x 10^{-6} in/in/°F
α 22	16.0 x 10^{-6} in/in/°F	-0.238 x 10^{-6} in/in/°F
E11	58.0 Msi	20.2 Msi
E22	1.0 Msi	20.2 Msi
G12	0.6 Msi	7.61 Msi
V12	0.30	0.30
ρ		.065 lbs/cu in

Property	T50/934 Laminate	T50/934 Lay-up(-60,60, 0, 0, 60, -60)
α 11	0.05 x 10^{-6} in/in/°F	4.73 x 10^{-6} in/in/°F
α 22	16.0 x 10^{-6} in/in/°F	4.73 x 10^{-6} in/in/°F
E11	37.0 Msi	16.7 Msi
E22	1.3 Msi	16.7 Msi
G12	0.66 Msi	5.76 Msi
V12	0.31	0.31
ρ		.05 lbs/ cu in

Al 7075-T651	
α	12 x 10^{-6} in/in/°F
E	10.3 Msi
G	3.9 Msi
V	.33

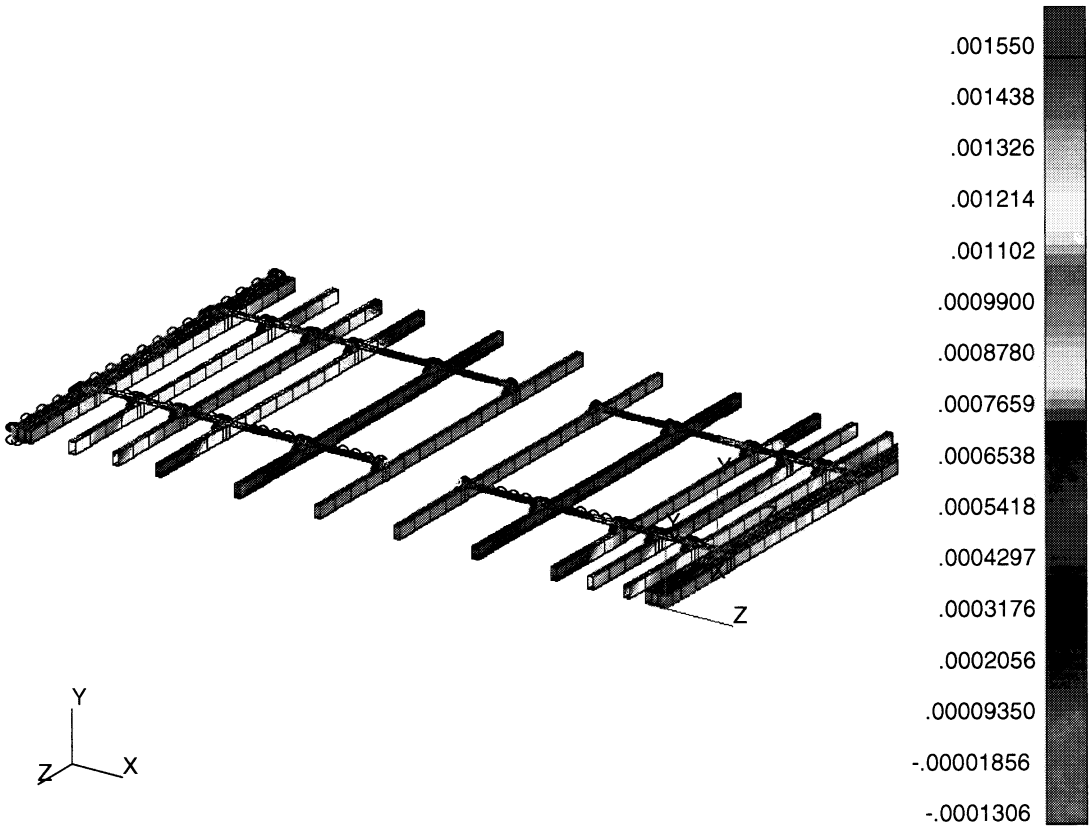

Figure 26. Transient Y-deflections (inches) for XN70 Antenna Array (β 60 orbit)

Conclusions

Using electronically integrated three-dimensional analysis modeling software (MSC/PATRAN), thermal analyzers (SINDA-85, TRASYS, P/Thermal), and structural analysis software (MSC/NASTRAN), parametric analyses of a 16-element waveguide space radiometer array were performed. Several surface coatings, several base materials, and two orbital extreme cases were analyzed, both for transient and orbit-average behavior. The orbit altitude was evaluated and found to have little impact on the results. The results of the analyses showed that the β 60 orbit produced the worst-case thermal transient, while the β 90 orbit produced the worst thermal gradient. Limited optimization of the surface coating layout was achieved with a combination of Al, Al-SiO2 MLI and Kapton MKI materials. It was shown that thermal gradients across the array were reduced significantly by use of a high conductivity XN70 carbon-reinforced polycyanate composite as compared to a standard graphite-epoxy (T50/934) and aluminum alloy 7075. The requirements on maintenance of orientation and position for the array are difficult to meet for an array of this size. The integrated analysis resulted in significant reduction of thermally driven deformations using the XN70 material. It was demonstrated that parametric studies and optimization of complex space arrays seeking minimum distortion can be accomplished using integrated thermal/structural techniques. A methodology for future improved optimization is identified.

Acronyms

AgTFE	Silver-Teflon
CTE	Coefficient of Thermal Expansion
ESTAR	Electronically Scanned Thinned Array Radiometer

MLI	Multi-layer Insulation
RBE2	Rigid Body Element (Form 2)
SOAP	Sun-synchronous Orbit Analysis Program
VDA	Vapor deposited aluminum
WG	Waveguide

References

[1] LeVine, D.M., Wilheit, T.T. Jr., Murphy, R.E. ,and Swift, C.T. , "A Multifrequency Microwave Radiometer of the Future," *IEEE Trans. Geosci. Remote Sensing*, Vol. 27, No. 2, pp. 193-199, March 1989.

[2] Jackson, T.J., *et.al.*, "Soil Moisture and Rainfall Estimation Over a Semiarid Environment with the ESTAR Microwave Radiometer," *IEEE Trans. Geosci. Remote Sensing*, Vol. 31, No. 4, pp. 836-841, July 1993.

[3] Fujioka, J.K. and Ely, W., *Development of the SEASAT-A Satellite Scatterometer Antenna*, NASA Contractor Report 145299, February 1978.

[4] LeVine, D.M., *ICESTAR: A Microwave Radiometer to Support Arctic Navigation and Polar Process Studies*, NASA Goddard Space Flight Center white paper, January 1994.

[5] Mutton, P., *et. al., A Conceptual Study for a Two-Dimensional, Electronically Scanned Thinned Array Radiometer*, NASA TM-109051, November, 1993.

[6] Gould, D. C., *A Conceptual Thermal Design Study of an Electronically Scanned Thinned Array Radiometer*, NASA TM-110173, May 1995.

[7] Birky, A.K., *et.al, Hydrostar Engineering Feasibility Report*, Swales and Associates for NASA GSFC, February 2, 1995.

[8] Le Vine, D.M. and Weissman, D.E., "Calibration of Synthetic Aperture Radiometers in Space: Antenna Effects", Proc. IGARSS-96, Vol II, pp. 878-880, Lincoln, Nebraska, May 1996.

[9] Tanner, A.., Swift, C., "Calibration of a Synthetic Aperture Radiometer," *IEEE Trans. Geo. and Remote Sens.*, Vol 31, No. 1, pp. 257-267, January 1993.

[10] Killough, B. D., *Thermal and Orbital Analysis of Earth Monitoring Sun-Synchronous Space Experiments*, NASA TM-101630, May 1990.

[11] Thermal Radiation Analyzer System (TRASYS) User's Manual, JSC-22964, April 1988.

[12] SINDA '85/FLUINT, Systems Improved Numerical Differencing Analyzer and Fluid Integrator, Version 2.3, MCR-90-512, August 1986.

[13] MSC/PATRAN User Manual, MacNeal-Schwendler Corporation, Version 5.0 (March 1996) and 6.0 (August 1996).

[14] Silverman, E. M. (Compiler), Composite Structures Design Guide, NASA Contractor Report 4708, March 1996.

[15] Parametric Technology Corporation, Pro/Mechanica Reference Manual, 1997.

REPORT DOCUMENTATION PAGE

Form Approved
OMB No. 0704-0188

1. AGENCY USE ONLY (*Leave blank*)	2. REPORT DATE	3. REPORT TYPE AND DATES COVERED
	February 1998	Technical Memorandum

4. TITLE AND SUBTITLE
Hydrostar Thermal and Structural Deformation Analyses of Antenna Array Concept

5. FUNDING NUMBERS
632-10-14-37

6. AUTHOR(S)
Ruth M. Amundsen, Drew J. Hope

7. PERFORMING ORGANIZATION NAME(S) AND ADDRESS(ES)
NASA Langley Research Center
Hampton, VA 23681-2199

8. PERFORMING ORGANIZATION REPORT NUMBER
L-17679

9. SPONSORING/MONITORING AGENCY NAME(S) AND ADDRESS(ES)
National Aeronautics and Space Administration
Washington, DC 20546-0001

10. SPONSORING/MONITORING AGENCY REPORT NUMBER
NASA/TM-1998-206288

11. SUPPLEMENTARY NOTES

12a. DISTRIBUTION/AVAILABILITY STATEMENT
Unclassified-Unlimited
Subject Category 18 Distribution: Standard
Availability: NASA CASI (301) 621-0390

12b. DISTRIBUTION CODE

13. ABSTRACT (*Maximum 200 words*)
The proposed Hydrostar mission used a large orbiting antenna array to demonstrate synthetic aperture technology in space while obtaining global soil moisture data. In order to produce accurate data, the array was required to remain as close as possible to its perfectly aligned placement while undergoing the mechanical and thermal stresses induced by orbital changes. Thermal and structural analyses for a design concept of this antenna array were performed. The thermal analysis included orbital radiation calculations, as well as parametric studies of orbit altitude, material properties and coating types. The thermal results included predicted thermal distributions over the array for several cases. The structural analysis provided thermally-driven deflections based on these cases, as well as based on a 1-g inertial load. In order to minimize the deflections of the array in orbit, the use of XN70, a carbon-reinforced polycyanate composite, was recommended.

14. SUBJECT TERMS
thermal, structural, analysis, thinned array, antenna, orbiting antenna, soil moisture, synthetic aperture technology, space, composite waveguide

15. NUMBER OF PAGES
28

16. PRICE CODE
A03

17. SECURITY CLASSIFICATION OF REPORT	18. SECURITY CLASSIFICATION OF THIS PAGE	19. SECURITY CLASSIFICATION OF ABSTRACT	20. LIMITATION OF ABSTRACT
Unclassified	Unclassified	Unclassified	